EFA 104448
18 February 2020
ARTICLE IN PRESS
No. of Pages 19, Model 3G

Engineering Failure Analysis xxx (xxxx) xxx

Contents lists available at ScienceDirect

Engineering Failure Analysis

journal homepage: www.elsevier.com/locate/engfailanal

# The behaviour of fibre-reinforced composites subjected to a soft impact-loading: An experimental and numerical study

Haibao Liu [a], Jun Liu [a], Cihan Kaboglu [a], Jin Zhou [b], Xiangshao Kong [c], Bamber R.K. Blackman [a], Anthony J. Kinloch [a,*], John P. Dear [a,*]

[a] *Department of Mechanical Engineering, Imperial College London, South Kensington Campus, London SW7 2AZ, UK*
[b] *School of Mechanical Engineering, Xi'an Jiaotong University, Xi'an 710049, People's Republic of China*
[c] *Departments of Naval Architecture, Ocean and Structural Engineering, School of Transportation, Wuhan University of Technology, Wuhan, Hubei 430063, People's Republic of China*

A R T I C L E  I N F O

*Article history:*
Received 17 December 2019
Accepted 11 February 2020
Available online xxxx

*Keywords:*
Composite laminates
Soft impact
Digital Image Correlation (DIC)
Numerical modelling

A B S T R A C T

The present paper presents experimental and numerical studies on the behaviour of composite laminates subject to impact loading by soft projectiles to represent the impact of a small bird or hail-stone. In this research, gas-gun experiments are performed to study woven carbon-fibre reinforced poly (ether-ether ketone) (CF/PEEK) composites subjected to an impact by soft-gelatine projectiles. In addition, woven carbon-fibre reinforced epoxy (CF/epoxy) composite specimens are also evaluated using gelatine projectiles to investigate the effect of the matrix system on the impact response of the composites. A high-speed camera is employed to capture the deformation of the projectiles and a three-dimensional (3D) Digital Image Correlation (DIC) system is used to record the deformation of the impacted composite specimens. A Finite Element (FE) model is developed to simulate the impact by a soft projectile on the composite specimens. Good agreement is shown between the predictions from using the FE model and the experimental results.



## 1. Introduction

With their increasing application in load-bearing structures, polymer-matrix fibre-reinforced composite materials have attracted much attention from both academia and industry. With an appropriate lay-up, such composites can possess excellent in-plane properties [1–5]. However, the effect of impact loading, e.g. by a high-velocity soft-impact, on the residual through-thickness properties is still a key safety concern for composite structures [6–9]. With this in mind, gas-gun impact experiments have been widely used to evaluate the reliability of composite structures and components. Indeed, a number of researchers have investigated the behaviour of composites subjected to impact loading by soft-body projectiles.

For example, Heimbs and Bergmann [10] conducted an experimental study on the response of composite specimens under high-velocity impact loading by soft-body gelatine projectiles. In their experiments, the composites were subjected to tensile or compressive loading before the impact experiments, to represent the loading conditions of aircraft structures when subjected to foreign-object impact by a soft body. The effect of pre-load was to modify the force-displacement response, and related stiffness of the panel, with a subsequent increase of damage. Zbrowski [11] performed soft-body impact tests on the elements of a composite tail-plane component using a gas-gun system. The soft projectile was again

* Corresponding authors.
*E-mail address:* j.dear@imperial.ac.uk (J.P. Dear).

https://doi.org/10.1016/j.engfailanal.2020.104448
1350-6307/© 2020 Published by Elsevier Ltd.



Please cite this article as: H. Liu, J. Liu, C. Kaboglu et al., The behaviour of fibre-reinforced composites subjected to a soft impact-loading: An experimental and numerical study, Engineering Failure Analysis, https://doi.org/10.1016/j.engfailanal.2020.104448

made of gelatine. The head-on and off-centre collisions on elements of the tail-plane were studied using two high-speed cameras to record the interaction between the projectile and the composite component. Damage inspection of the tested components showed that the head-on collision significantly damaged the vertical tail-plane, but the off-centre collision caused only minor permanent deformation and, importantly, did not damage the leading edge of the component. Johnson and Holzapfel [12] employed finite element (FE) analysis codes to simulate the soft impact on the composite shell structures. The intralaminar and interlaminar damage models were developed and implemented in commercial explicit FE codes. The developed composites failure models and code were applied to simulate soft impact on idealised aerostructures. The predictive capability of the developed models were discussed for capturing the loading response of composite aircraft structures subjected to deformable soft body impact.

In the present research, the results from a fundamental experimental and numerical study on the impact behaviour of composite laminates subjected to a soft-body impact are presented. For the experimental studies, a well-defined manufacturing process, which is easy to perform and control, is developed for the preparation of the gelatine projectiles. These gelatine projectiles are subsequently employed to perform gas-gun impact tests on the composite laminates which act as the target specimens. A thermoplastic polymer-matrix composite (i.e. a reinforced poly (ether-ether ketone) (CF/PEEK) composite) and a thermoset polymer-matrix composite (i.e. a carbon-fibre reinforced epoxy (CF/epoxy) composite) are studied and compared to investigate the effect of the matrix system on the impact response. A high-speed camera is employed to capture the deformation and flow of the gelatine projectiles during the test and the deformations undergone by the composite specimens are recorded using a three-dimensional (3D) Digital Image Correlation (DIC) system. For the numerical studies, a FE model is developed, using the 'Abaqus/Explicit 2017' software code, to model the soft impact on the composites. The model implemented in the FE code for predicting the initiation of intralaminar damage in the fibre-reinforced composites is based upon the Hashin damage approach [13–15], which has a higher computational efficiency than other possible sub-routine damage models, and for predicting the initiation of interlaminar damage is based upon the Abaqus in-built cohesive solution [15–17]. The evolution of the damage during the impact event is then also predicted by implementing damage evolution laws in the FE code as a sub-routine. The interlaminar damage evolution law is based on a linear-softening material model embedded into a bilinear cohesive law. The soft-gelatine projectile is modelled using the Smoothed Particle Hydrodynamics (SPH) technique [18]. The modelling results, including predictions of (a) the deformation and flow of the projectile, (b) the deformation of the impacted composite and (c) the location and extent of the damage suffered by the composite, are then compared with the corresponding experimental results. In this paper, the focus of the research presented, has been to study soft impact on woven carbon fibre composites employing PEEK and epoxy as matrix materials and develop SPH models to describe the impact process and damage generated.

## 2. The modelling approach

### 2.1. Modelling the response of the projectile

The SPH approach [18] was employed to model the behaviour of the gelatine projectile within the 'Abaqus/Explicit 2017' code, as discussed later. For the SPH method to capture the response of the soft-gelatine projectile upon impact of the composite, a constitutive law is required with suitable material properties employed for the gelatine projectile. The model used was originally developed for ballistic impact in metals and describes an isotropic elastic-plastic material subjected to relatively low pressures with an equation of state (EOS) describing the hydrodynamic pressure versus volume behaviour at high pressures. The linear Mie-Grüneisen EOS was employed to define the coupled equations for pressure and internal energy [15]. The most common form for this EOS is given by:

$$p - p_H = \Gamma \rho (E_m - E_H) \quad (1)$$

where $p$ is the pressure which is defined as positive in compression. The Hugoniot pressure, $p_H$, is a function only of the density and can be ascertained from fitting to the experimental data. The parameters $E_m$ and $E_H$ are the internal energy per unit mass and the specific energy per unit mass (i.e. the Hugoniot energy), respectively. The parameter, $\rho$, is the current density of the gelatine projectile. The parameter, $\Gamma$, is the Grüneisen ratio and is defined by:

$$\Gamma = \Gamma_0 \frac{\rho_0}{\rho} \quad (2)$$

where $\Gamma_0$ is a material constant and $\rho_0$ is the reference density of the gelatine projectile. The specific energy per unit mass, $E_H$, is related to the Hugoniot pressure by:

$$E_H = \frac{p_H \eta}{2\rho_0} \quad (3)$$

where $\eta = 1 - \rho_0/\rho$ and $\eta$ is the nominal volumetric compressive strain. The elimination of $\Gamma$ and $E_H$ from the above equations yields:

$$p = p_H\left(1 - \frac{\Gamma_0 \eta}{2}\right) + \Gamma_0 \rho_0 E_m \quad (4)$$



Please cite this article as: H. Liu, J. Liu, C. Kaboglu et al., The behaviour of fibre-reinforced composites subjected to a soft impact-loading: An experimental and numerical study, Engineering Failure Analysis, https://doi.org/10.1016/j.engfailanal.2020.104448

In the above equation, the pressure, $p$, is a function of the Hugoniot pressure, $p_H$, and the nominal volumetric compressive strain, $\eta$. Once the relationship between $p_H$ and $\eta$ is defined, the pressure, $p$, can be expressed as a single-variable function. To achieve this, the linear $U_s$ versus $U_p$ relationship was employed to fit the curve of the Hugoniot pressure versus the nominal volumetric compressive strain. The term $U_s$ is the shock-wave velocity. The term $U_p$ is the particle velocity of the projectile and the measured value of $U_p$ was assigned to all the 8-node linear-brick (C3D8R) elements when the FE model was started, as discussed in detail later. However, immediately after initial contact of the projectile with the composite, these elements for the projectile were converted to continuum particle (PC3D) elements and the value of $U_p$ assigned to the particle elements was then continually updated based upon the loading conditions on the particles after the initial contact. Assuming the usual linear $U_s$ versus $U_p$ relationship, then the Hugoniot pressure versus the nominal volumetric compressive strain equation is given by:

$$p_H = \frac{\rho_0 c_0^2 \eta}{(1 - s\eta)^2} \tag{5}$$

where the fitting coefficient, $s$, is the slope of the linear relationship between $U_s$ and $U_p$:

$$U_s = c_0 + sU_p \tag{6}$$

where $c_0$ is the reference speed of sound in the gelatine projectile. With the above assumptions, the relationship between the pressure, $p$, and the nominal volumetric compressive strain, $\eta$ may now be written as:

$$p = \frac{\rho_0 c_0^2 \eta}{(1 - s\eta)^2}\left(1 - \frac{\Gamma_0 \eta}{2}\right) + \Gamma_0 \rho_0 E_m \tag{7}$$

Thus, in the FE model, see below, Eqs. (5) and (6) were employed to define the parameters in the EOS for modelling the gelatine projectile and Eq. (7) was used to predict the contact pressure between the gelatine projectile and the composite.

### *2.2. Modelling the response of the composites*

#### *2.2.1. The intralaminar damage model*

The model for predicting the initiation of any intralaminar damage was implemented within the 'Abaqus/Explicit 2017' FE code, as discussed later, and was based upon Hashin's theory [13–15]. In Hashin's damage model, four different types of damage mechanisms, which arise from tensile fibre failure, compressive fibre failure, tensile matrix failure and compressive matrix failure, are employed to capture the initiation of intralaminar damage in the unidirectional-fibre sub-plies. The material coordinate system in the unidirectional-fibre sub-ply was defined as the 1-2-3 coordinate system, where the longitudinal fibre-direction is defined as the 11-direction and the transverse direction, perpendicular to the longitudinal fibre-direction, was defined as the 22-direction. The general forms of the damage criteria in Hashin's approach to model the initiation of the above four different types of damage are given as:

$$\text{Tensile fibre failure } (\hat{\sigma}_{11} \geq 0): \quad F_f^t = \left(\frac{\hat{\sigma}_{11}}{X^T}\right)^2 \tag{8}$$

$$\text{Compressive fibre failure } (\hat{\sigma}_{11} < 0): \quad F_f^c = \left(\frac{\hat{\sigma}_{11}}{X^C}\right)^2 \tag{9}$$

$$\text{Tensile matrix failure } (\hat{\sigma}_{22} \geq 0): \quad F_m^t = \left(\frac{\hat{\sigma}_{22}}{Y^T}\right)^2 \tag{10}$$

$$\text{Compressive matrix failure } (\hat{\sigma}_{22} < 0): \quad F_m^c = \left(\frac{\hat{\sigma}_{22}}{2S^T}\right)^2 + \left[\left(\frac{Y^C}{2S^T}\right)^2 - 1\right]\frac{\hat{\sigma}_{22}}{Y^C} + \left(\frac{\hat{\tau}_{12}}{S^L}\right)^2 \tag{11}$$

In the above equations, the indices on the terms $F_f^t$, $F_f^c$, $F_m^t$ and $F_m^c$ represent the four types of damage of tensile fibre failure, compressive fibre failure, tensile matrix failure and compressive matrix failure, respectively, and failure is predicted to occur when $F \geq 1$. The parameters, $X^T$ and $X^C$ denote the tensile and compressive strengths in the longitudinal fibre-direction, respectively. The terms $Y^T$ and $Y^C$ are the tensile and compressive strengths in the transverse direction, respectively; $S^L$ and $S^T = Y^C/2$ denote the shear strengths in the longitudinal and transverse directions to the fibres, respectively; and the term $\hat{\sigma}_{11}$, $\hat{\sigma}_{22}$ and $\hat{\tau}_{12}$ are components of the effective stress tensor, $\hat{\sigma}$, that are used to evaluate the above criteria. The compressive matrix failure criterion employed is based on a quadratic expression which incorporates stress interactions and this can be traced back to the von Mises yield criteria.



Please cite this article as: H. Liu, J. Liu, C. Kaboglu et al., The behaviour of fibre-reinforced composites subjected to a soft impact-loading: An experimental and numerical study, Engineering Failure Analysis, https://doi.org/10.1016/j.engfailanal.2020.104448

Corresponding to the damage initiation mechanisms defined in Hashin's criteria, four damage parameters, $d_f^t$, $d_f^c$, $d_m^t$ and $d_m^c$, were implemented in the damage evolution model. A general form of the damage variable for a particular damage initiation mechanism is given by [15]:

$$d = \frac{\varepsilon^f(\varepsilon - \varepsilon^0)}{\varepsilon(\varepsilon^f - \varepsilon^0)} \tag{12}$$

where $d = d_f^t$ represents fibre tension failure, $d = d_f^c$ represents fibre compression failure, $d = d_m^t$ represents matrix tension failure and $d = d_m^c$ represents matrix failure, respectively. The strain, $\varepsilon$, is the equivalent strain in the composite ply. The strain values, $\varepsilon^0$ and $\varepsilon^f$, are the equivalent strains corresponding to the initiation of failure and final failure, respectively. For fibre tension or fibre compression failure, the terms $\varepsilon$, $\varepsilon^0$ and $\varepsilon^f$ are assigned to be $\varepsilon = \varepsilon_{11}$, $\varepsilon^0 = \varepsilon_{11}^0$ and $\varepsilon^f = \varepsilon_{11}^f$, respectively. For tensile or compressive matrix failure, the terms $\varepsilon$, $\varepsilon^0$ and $\varepsilon^f$ are assigned to be $\varepsilon = \varepsilon_{22}$, $\varepsilon^0 = \varepsilon_{22}^0$ and $\varepsilon^f = \varepsilon_{22}^f$, respectively. In the damage evolution model, the values of the initial failure strains, $\varepsilon^0$, are equal to the strain values corresponding to damage initiation, which may be directly obtained from the computation via implementing Eqs. (8) to (11), respectively. The final failure strains may be determined from a knowledge of the tensile, $G_{Ic}|_{ft}$, and compressive, $G_{Ic}|_{fc}$, intralaminar ply fracture energies in the longitudinal fibre-direction, and the tensile, $G_{Ic}|_{mt}$, and compressive, $G_{Ic}|_{mc}$, interlaminar ply fracture energies in the transverse to the fibre-direction.

Three damage variables, $d_f$, $d_m$ and $d_s$, which reflect fibre damage, matrix damage and shear damage, respectively, were derived from the damage parameters, $d_f^t$, $d_f^c$, $d_m^t$ and $d_m^c$, as follows:

$$\text{For fibre damage:} \quad d_f = \begin{cases} d_f^t & \hat{\sigma}_{11} \\ d_f^c & \hat{\sigma}_{11} \end{cases} \tag{13}$$

$$\text{For matrix damage:} \quad d_m = \begin{cases} d_m^t & \hat{\sigma}_{22} \\ d_m^c, & \hat{\sigma}_{22} \end{cases} \tag{14}$$

$$\text{For shear damage:} \quad d_s = 1 - \left(1 - d_f^t\right)\left(1 - d_f^c\right)\left(1 - d_m^t\right)\left(1 - d_m^c\right) \tag{15}$$

During the evolution of damage, the derived damage variables, $d_f$, $d_m$ and $d_s$, were employed to update the stiffness matrix of the composite ply and to compute the degraded stresses that were acting. For more details, refer to the Abaqus 2017 documentation [15].

### 2.2.2. The interlaminar damage model

The initiation of any interlaminar damage in the composite laminates was captured by using a quadratic-stress criterion, which was implemented within the FE code, as discussed later, and is given by [15–17]:

$$\left(\frac{\langle t_{33}\rangle}{t_{33}^0}\right)^2 + \left(\frac{t_{31}}{t_{31}^0}\right)^2 + \left(\frac{t_{32}}{t_{32}^0}\right)^2 \geq 1 \tag{16}$$

where $t_i (i = 33, 31, 32)$ represent the current normal and shear stresses, and $t_i^0 (i = 33, 31, 32)$ represent the normal and shear cohesive-law strengths, when the separation is either purely normal (i.e. the 33) direction to the interface, or purely in the first shear (i.e. 31), or the second shear (i.e. 32) directions, respectively. The interlaminar damage is assumed to initiate when the above quadratic interaction function, involving the ratios of the stresses, reaches a value of one. Thus, employing Eq. (16), the value of the displacement, $\delta^o$, at the initiation of damage may be deduced.

The evolution of interlaminar damage during the impact event was modelled using a linear-softening material model embedded into a bilinear surface cohesive law, where the traction is plotted versus the displacement, $\delta$. This was implemented as a sub-routine in the FE code [15–17]. This embedded interface element requires a value of the interlaminar fracture energy, $G_c$, and this represents the area under the bilinear cohesive law. The energy-based Benzeggagh-Kenane (B-K) [15] criterion for Mixed-mode propagation was used to derive a value $G_c$ for the growth of the delamination between the composite plies, as given by:

$$G_c = G_{Ic} + (G_{IIc} - G_{Ic})\left[\frac{G_{II}}{G_I + G_{II}}\right]^\eta \tag{17}$$

where $G_{Ic}$ is the Mode I (opening tensile) interlaminar facture energy, $G_{IIc}$ is the Mode II (in-plane shear) interlaminar facture energy and $\eta$ is the B-K Mixed-mode interaction exponent, which may all be experimentally measured. The parameters $G_I$ and $G_{II}$ are the current Mode I and Mode II energy-release rates, respectively, as calculated from the FE code. Complete fracture of the interface element was assumed to occur, and delamination results, when the cohesive traction vanishes at the end of the degradation step. That is when the displacement, $\delta$, of the interface element, as determined in the FE code, attains the criterion:

$$\delta \geq \delta^f \tag{18}$$

where $\delta^f$ is the displacement of the interface element at failure.

## 3. The projectiles and composites

### 3.1. The projectiles

A well-defined process, which is relatively simple and controllable, has been developed for preparing the soft-gelatine projectiles to a uniform standard. The ingredients used to prepare these projectiles were gelatine powder and distilled water. The gelatine powder was supplied by Honeywell Specialty, Germany. The detailed procedure, to manufacture the gelatine projectiles, is presented in Table 1. The gelatine projectiles had a nominal diameter of 23 mm and a nominal length of 45 mm. The photograph of a typical gelatine projectile is given in Fig. 1 and Table 2 shows the dimensions of the gelatine projectiles [18]. Due to their relatively low hardness, the gelatine projectiles initially tended to deform during the launching event from the gas-gun. To eliminate this problem, a plastic sabot was developed to maintain the shape of the gelatine projectile during the acceleration phase of the impact tests. The unassembled and assembled projectile-sabot system is shown in Fig. 2.

### 3.2. Composite specimens

A woven T300 carbon-fibre reinforced PEEK composite and a woven T300 carbon-fibre reinforced 'Toray 3631' epoxy composite were studied. The woven carbon-fibre ply possessed a [0–90°] architecture. These materials were supplied by Haufler Composites, Germany. An Out-of-Autoclave (OOA) manufacturing route was employed to consolidate the CF/PEEK prepregs and an autoclave was used to cure the CF/epoxy prepregs. Diagrams of the processing schedules for the CF/PEEK prepregs and the CF/epoxy prepregs are shown in Fig. 3a and b, respectively. Composite target test specimens were machined from the composite panels using a diamond saw and a floor-standing drill. The lay-up employed for the woven CF/PEEK and woven CF/epoxy composites was $[0\text{–}90^\circ]_{4s}$ and the nominal thickness of the manufactured specimens was 2 mm. The geometry of the composite target test specimens for the impact tests is given in Fig. 4. Table 3 gives all the dimensions of the specimens, where $H$ and $W$ are the specimen height and width, respectively. The length, $d_3$, defines the size of the DIC pattern area. The length, $d_1$, defines the distance between the sample edge and the centre line of the holes and $d_2$ defines the distance between each of the holes. The radius of each hole is $R$. For the DIC measurement, the specimens were first painted on the rear-face using a white matt paint and then 'speckled' using a paintbrush to form the matt-black pattern.

## 4. Experimental investigations

### 4.1. The gas-gun experiments

A helium-propellant gas-gun, which has a four-litre pressure vessel and a three-metre-long barrel, was employed to accelerate the projectiles in the impact tests. The velocity of the projectile was adjusted by changing the pressure of the vessel. The incident velocity of the projectiles was measured using two pairs of infrared sensors located at the end of the barrel. A new projectile and a new sabot were employed for each impact test. The schematic of the experimental set-up for the gas-gun experiments is shown in Fig. 5. During the experiments, the composite target specimen was fixed by a specimen support and this consisted of two main components: one component being the 20 mm thick steel supporting plate, which had a

**Table 1**
Detailed preparation procedure of the gelatine projectiles.

| Steps | Operations |
|---|---|
| I | Raise the temperature of the distilled water to 80 °C and maintain this temperature using a water bath with a thermocouple to monitor the temperature of the distilled water. |
| II | Mix the gelatine powder with distilled water at a mass ratio of 1:10, and then stir the mixture, using a magnetic stirrer, at a stirring rate of 50 rpm until the gelatine powder is completely dissolved. |
| III | Transfer the solution to a beaker and let the solution cool down to room temperature. |
| IV | Transfer the solution at room temperature to a poly(tetrafluoroethylene) (PTFE) cylindrical mould, which has a paraffin-oil coated onto its surface to prevent leakage and facilitate the subsequent removal of the solid gelatine projectile. |
| V | Seal the mould with cling film placed over the top of the mould to prevent dehydration. |
| VI | Place the sealed mould into an environmental chamber where the temperature is kept between 5 and 7 °C for at least 8 h. |
| VII | Carefully push the solid gelatine cylinder out from the mould and use a digitally controlled disc-saw to cut the gelatine cylinders to the required length for the projectiles. |



Please cite this article as: H. Liu, J. Liu, C. Kaboglu et al., The behaviour of fibre-reinforced composites subjected to a soft impact-loading: An experimental and numerical study, Engineering Failure Analysis, https://doi.org/10.1016/j.engfailanal.2020.104448

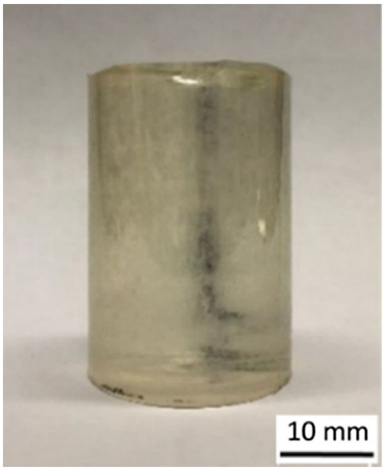


**Fig. 1.** The photograph of a gelatine projectile.

70 mm × 70 mm cut-out and the other component was the 15 mm thick steel clamping plate, which also had an opening of 70 mm × 70 mm.

### *4.2. Digital Image Correlation (DIC) measurements*

A 3D DIC system was used to measure the deformation of the rear-face of the specimens during impact loading. Two 'Phantom Miro M/R/LC310' high-speed cameras, supplied by Vision Research Phantom, USA, were employed. A pair of identical 'Nikon' lenses, with a fixed focal length of 50 mm, supplied by Nikon, UK, were used with these two cameras. During the tests, the recording rate of these two cameras was set at 40,000 frames per second and they were triggered simultaneously by the signal generated from the infrared sensors. To achieve the brightness required for the high-speed DIC measurements, two bright-light sources, which were only turned on a few seconds before the gas-gun was fired, were employed to illuminate the rear-face of the composite specimens, which were painted with matt white paints and speckled using black dots. The area of interest for the DIC measurement was 60 mm × 60 mm. It should be noted that the DIC technique only records surface displacements and strains but this is useful in recording the overall displacement response of the panel before damage and can detect surface damage when it occurs.

### *4.3. Damage inspection*

After the impact experiments, visual inspections were undertaken on the composite specimens and photographs were taken from the rear-faces of the post-impacted specimens. In general, the type of damage suffered by the composites on the rear-face could be categorised as: (a) no visible damage present, (b) cracking observed, (c) fracture having occurred, and (d) perforation (i.e. penetration of the projectile through the specimen) having occurred. The main difference between 'type (b) cracking' and 'type (c) fracture' is whether there was fibre breakage observed. For 'type (b) cracking' this was defined as when cracks were only observed in the matrix. However, for 'type (c) fracture', fibre failure was also observed. Schematics of these descriptions for status of the post-impacted composites are shown in Fig. 6.

## 5. Experimental results

### *5.1. Deformation of the gelatine projectile*

Fig. 7 shows the deformation of the gelatine projectile recorded by a high-speed camera during an impact with the CF/PEEK composite specimen for an impact energy of 37 J. Within the resolvable time intervals, the time, *t*, corresponding to the initial contact was defined as 0.0 ms, as shown in Fig. 7c. It was found that at the beginning of the impact event (i.e. t = 0.0 ms) the shape of the gelatine projectile was well preserved, which ensured that the gelatine projectile impacted

**Table 2**
Physical properties of the gelatine projectiles [18,36].

| Projectile | Density (g/cm$^3$) | Mass (g) | Diameter (mm) | Length (mm) |
|---|---|---|---|---|
| Gelatine | 1.06 ± 0.003 | 20 ± 0.5 | 23 ± 0.5 | 45 ± 0.5 |



Please cite this article as: H. Liu, J. Liu, C. Kaboglu et al., The behaviour of fibre-reinforced composites subjected to a soft impact-loading: An experimental and numerical study, Engineering Failure Analysis, https://doi.org/10.1016/j.engfailanal.2020.104448

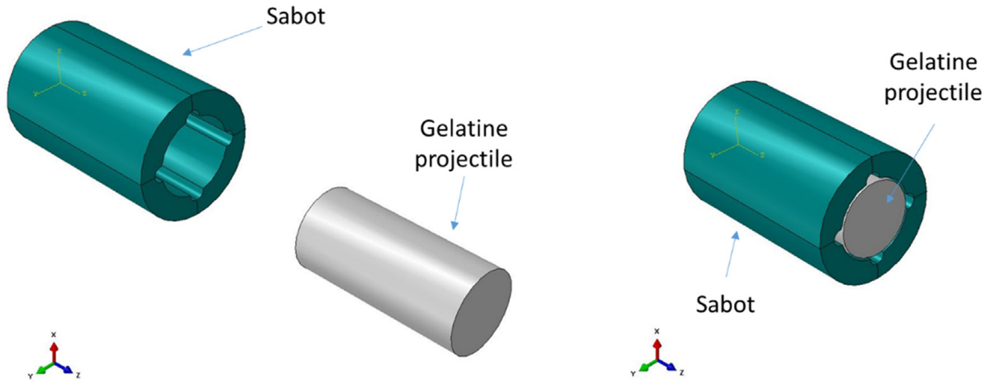


**Fig. 2.** Schematic of the disassembled (left) and assembled (right) projectile and sabot system.

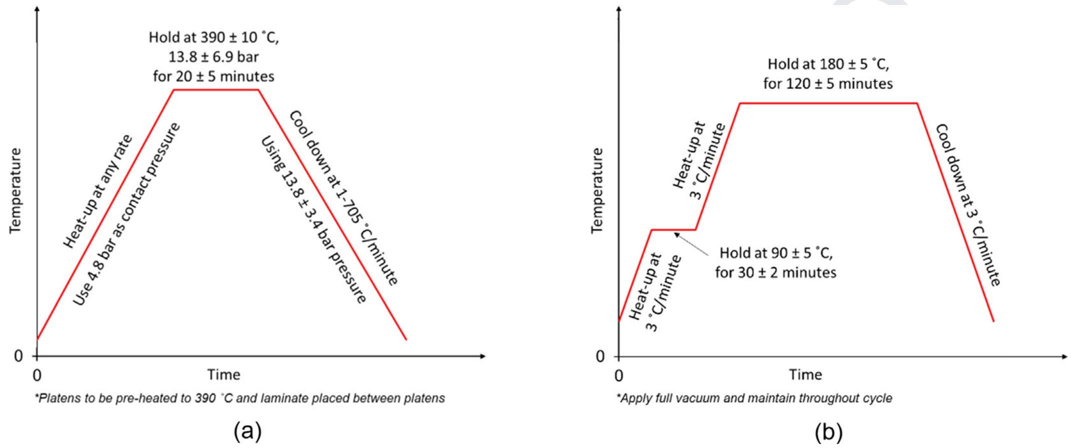


**Fig. 3.** Processing schedules for: (a) the CF/PEEK prepregs and (b) the CF/epoxy prepregs.

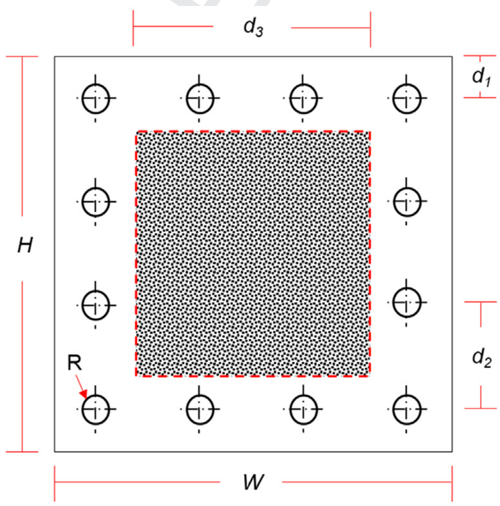


**Fig. 4.** Schematic drawing of the composite specimens.

**Table 3**
Dimensions of the composite target test specimens.

| Dimensions | $W$ (mm) | $H$ (mm) | $d_1$ (mm) | $d_2$ (mm) | $d_3$ (mm) | $R$ (mm) |
|---|---|---|---|---|---|---|
| Values | 140 | 140 | 16 | 36 | 70 | 5 |

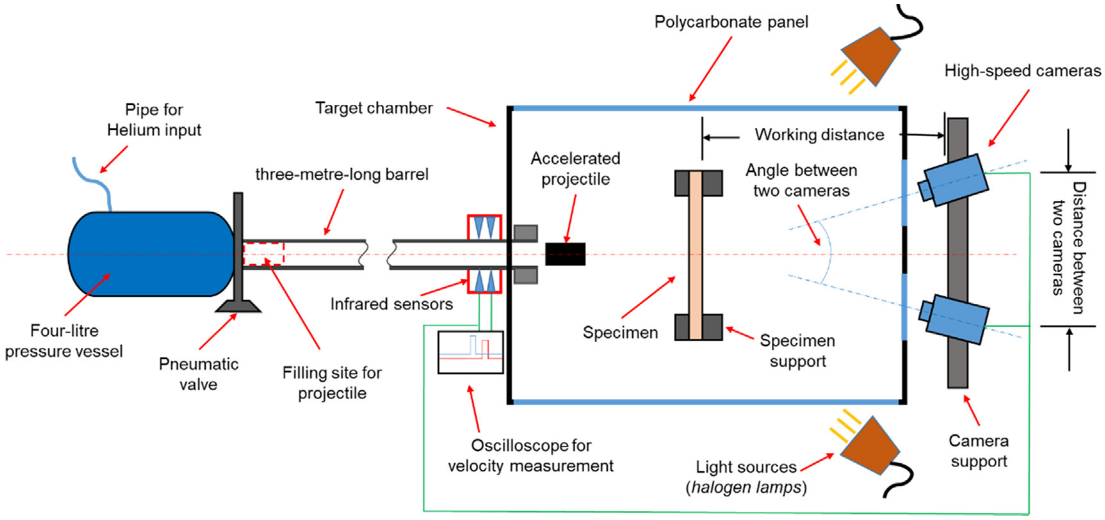


**Fig. 5.** Schematic of the experimental set-up for the gas-gun impact tests.

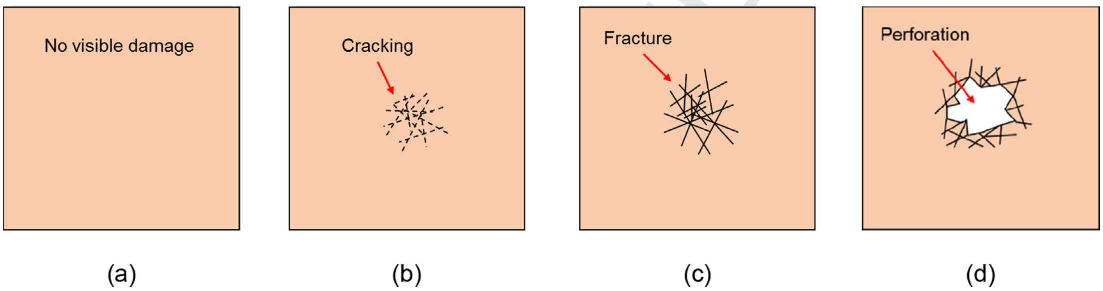


**Fig. 6.** Schematics of the types of post-impact damage on the rear-face of the composites: (a) no visible damage, (b) cracking, (c) fracture, and (d) perforation.

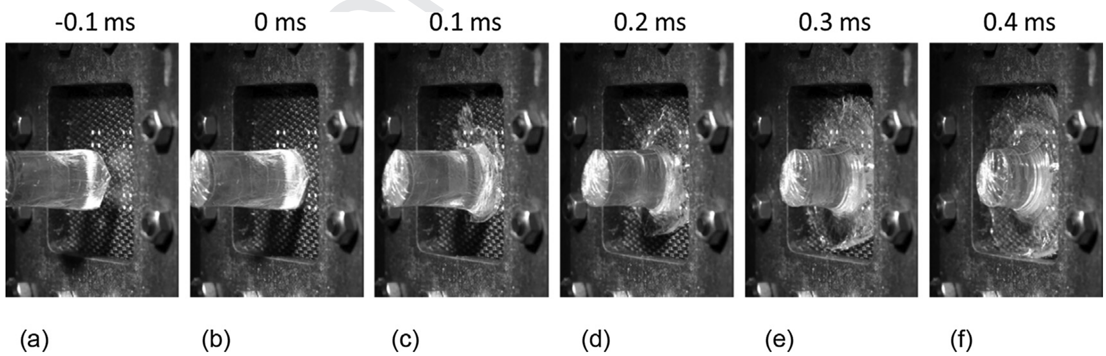


**Fig. 7.** Deformation history of the gelatine projectile for a 37 J impact energy impacting the CF/PEEK composite.

the centre of the specimen and then deformed symmetrically. However, in Fig. 7g for t = 0.4 ms, the gelatine projectile can clearly be seen to be flowing freely after impact.

### 5.2. Effects of the impact energy of the gelatine projectile

To study the effects of the impact energy on the response of the CF/PEEK composites subjected to soft impact-loading, these composites were impacted using gelatine projectiles fired at four different impact velocities, and hence with different impact energies. The testing configurations for investigating the effects of the impact energy on the impact response of the CF/PEEK specimens are given in Table 4.

#### 5.2.1. Comparison of the Digital Image Correlation (DIC) results

The 3D DIC system was employed to measure the major strain and out-of-plane (OOP) displacement on the rear-faces of the composites. The main DIC results obtained from the CF/PEEK composites, impacted by gelatine projectiles at different energy levels, are summarised in Table 5. (It should be noted that due to fracture of the rear-face during 'Test GCP-IV' when an energy level of 72 J was used, no accurate value for the maximum major strain could be obtained from the DIC results for this test.) As the impact energy is steadily increased, the maximum major strain and maximum OOP displacement both increased in value.

Figs. 8 and 9 present the typical DIC results obtained from the CF/PEEK composite impacted by a gelatine projectile with impact energy of 37 J. Fig. 8a shows the major strain maps, from which the evolution of the major strains along the horizontal mid-section, during the loading and unloading events, were also determined, Fig. 8b. It should be noted that the total loading time for the DIC maps was 0.175 ms, during which time the major strain increased from 0.0 to 0.013. The average strain-rate, $\dot{\varepsilon}$, is given by:

$$\dot{\varepsilon} = \frac{\Delta\varepsilon}{\Delta t} \quad (19)$$

with $\Delta\varepsilon$ and $\Delta t$ representing the strain and time increments, respectively. For the complete loading event, then $\Delta\varepsilon = 0.013$ and $\Delta t = 0.175$ ms, which gives the average strain rate, $\dot{\varepsilon}$, as 74.3 $s^{-1}$. (With respect to the numerical modelling studies discussed below, it should be noted that at this value of strain rate then significant rate effects have not been previously observed on the elastic and failure properties of such composites [20].) The OOP displacement contours, corresponding to different times during the impact tests, were also obtained from the DIC results and are shown in Fig. 9a for an impact energy of 37 J. Similarly, the OOP displacements along the horizontal mid-section, during the loading and unloading process of the specimen, were also obtained and are shown in Fig. 9b.

#### 5.2.2. Comparison of the post-impact damage

Representative photographs taken of the rear-faces of two of the gelatine-impacted CF/PEEK specimens are shown in Fig. 10, along with corresponding magnified images of the central area. In Fig. 10a, where the CF/PEEK composite was impacted by a gelatine projectile with energy of 37 J, no visible damage was observed. The same observation, of no visible damage, was recorded for the CF/PEEK tests conducted at impact energy levels of 53 J and 64 J. In contrast, the CF/PEEK composite impacted using a gelatine projectile with an impact energy of 72 J has suffered 'type (c)' fracture damage, with cracking in the matrix mainly being confined to the central area of the specimen, as shown in Fig. 10b. Further, obvious fibre

**Table 4**
Test configurations for investigating the effects of the impact velocity and energy on the CF/PEEK composites.

| Test | Projectile | Projectile mass (g) | Impact velocity (m/s) | Impact energy (J) |
|---|---|---|---|---|
| GCP-I | Gelatine | 20 ± 0.5 | 61 ± 2.5% | 37 ± 5% |
| GCP-II | Gelatine | 19 ± 0.5 | 75 ± 2.5% | 53 ± 5% |
| GCP-III | Gelatine | 20 ± 0.5 | 80 ± 2.5% | 64 ± 5% |
| GCP-IV | Gelatine | 20 ± 0.5 | 85 ± 2.5% | 72 ± 5% |

**Table 5**
Main DIC results for the CF/PEEK composites impacted by the gelatine projectiles.

| Test | Impact velocity (m/s) | Impact energy (J) | Maximum major strain | Maximum OOP displacement (mm) |
|---|---|---|---|---|
| GCP-I | 61 ± 2.5% | 37 ± 5% | 0.013 ± 3% | 3.9 ± 3% |
| GCP-II | 75 ± 2.5% | 53 ± 5% | 0.014 ± 3% | 4.2 ± 3% |
| GCP-III | 80 ± 2.5% | 64 ± 5% | 0.015 ± 3% | 4.6 ± 3% |
| GCP-IV | 85 ± 2.5% | 72 ± 5% | N/A | 4.8 ± 3% |

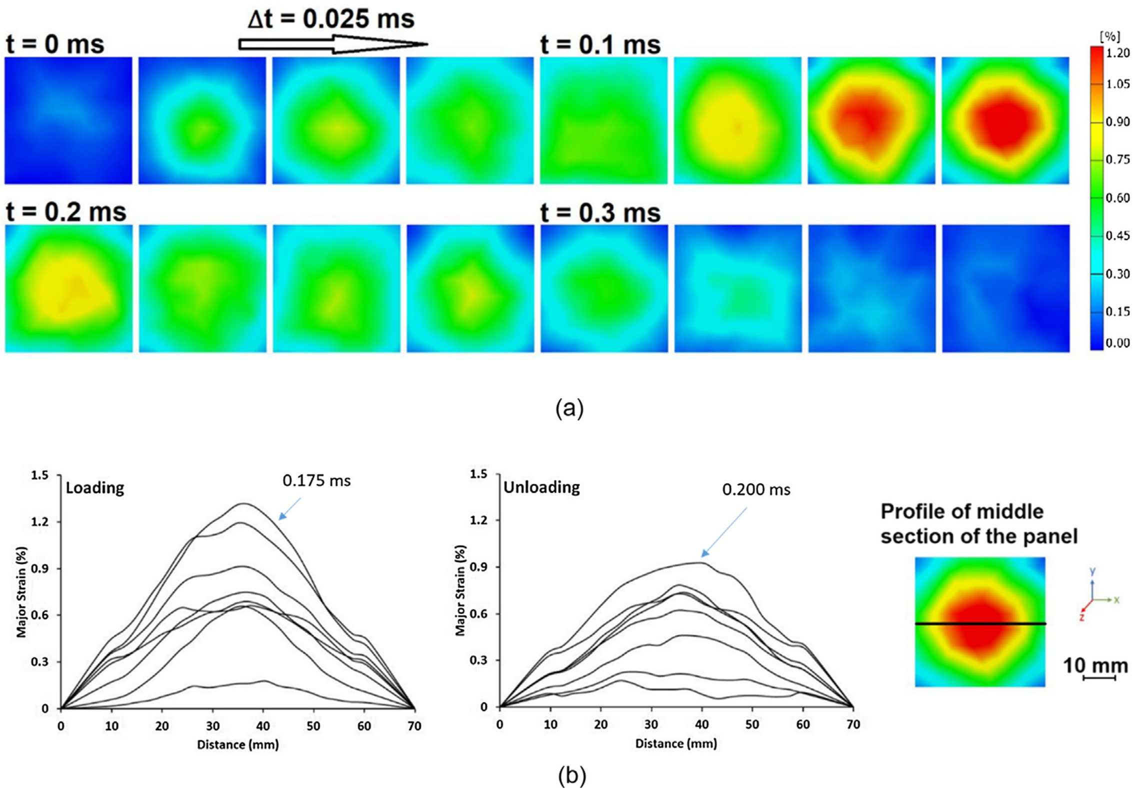


**Fig. 8.** CF/PEEK composites impacted at a 37 J energy level: (a) the major strain maps and (b) the evolution of the major strain profiles (in intervals of 0.025 ms) during loading and unloading. (Inset picture, on right, shows a horizontal solid line where the profile section is taken.)

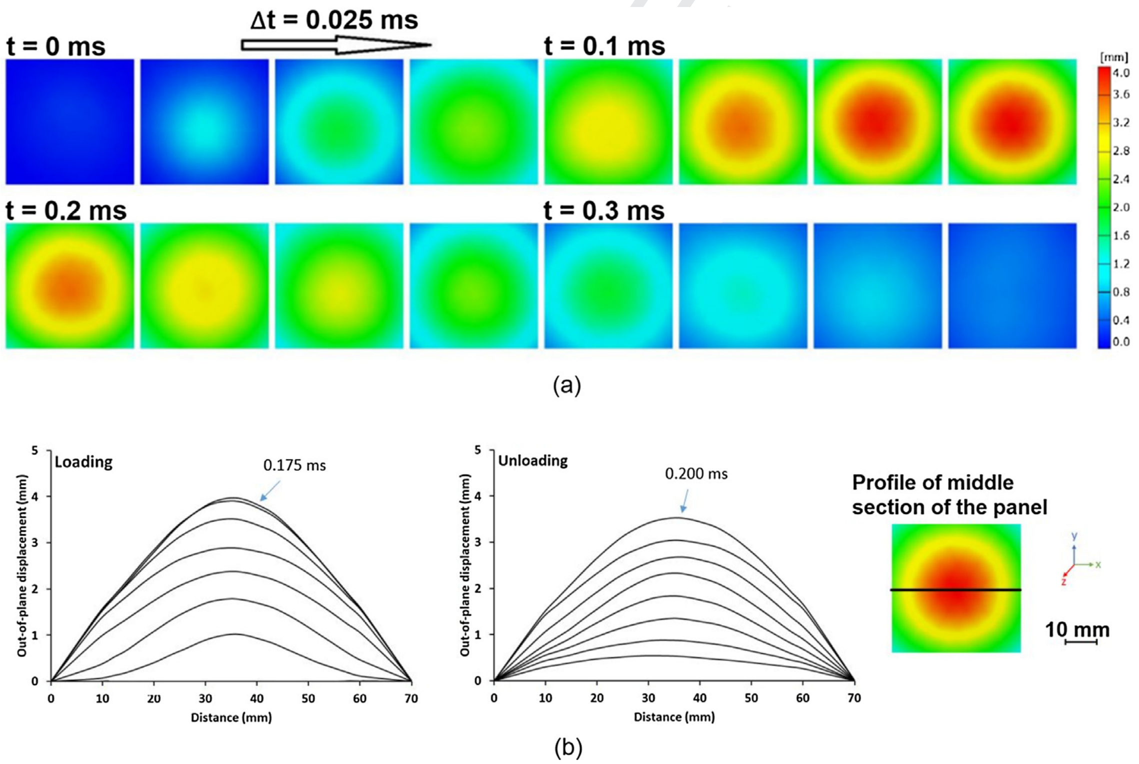


**Fig. 9.** CF/PEEK composites impacted at a 37 J energy level: (a) the OOP displacement contours and (b) the evolution of the OOP displacement profiles (in intervals of 0.025 ms) during loading and unloading. (Inset picture, on right, shows a horizontal solid line where the profile section is taken.)

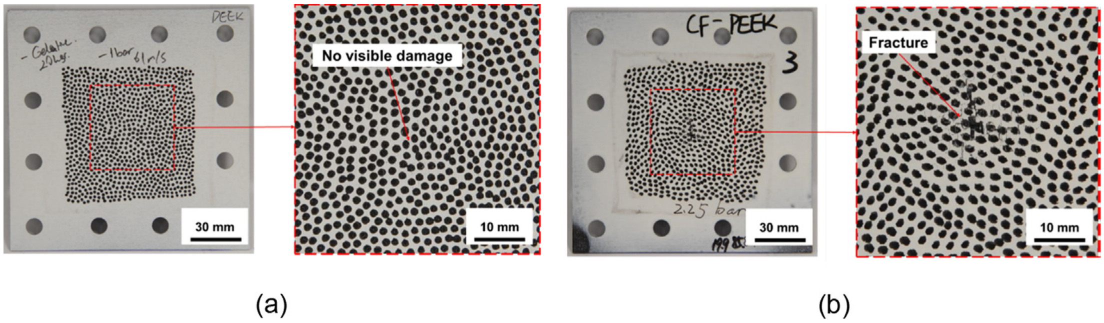


**Fig. 10.** Photographs of the rear-faces of the CF/PEEK composites after impact: (a) for an energy of 37 J ('Test GCP-I') and (b) for an energy of 72 J ('Test GCP-IV').

breakage was observed in this CF/PEEK composite specimen. Thus, it can be concluded that there is a critical impact energy between about 64 J and 72 J at which visible damage in the CF/PEEK composite is initiated.

### *5.3. Effects of the matrix system*

To study the effects of the employed matrix system on the impact response of the composite laminates, CF/epoxy composite specimens were also impacted, using a soft-gelatine projectile, at an energy level of 38 J. The details of the testing conditions are summarised in Table 6 and the results are shown in Table 7 and Fig. 11. As may be seen, the main effect of the matrix selected for the carbon-fibre composite is that the CF/PEEK composite ('Test GCP-I') impacted at an energy level of 37 J did not show any visible damage, whilst the CF/epoxy composite ('Test GCE-I') showed significant damage with 'type (b) cracking' being recorded.

**Table 6**
Gas-gun test conditions to study the effect of the matrix system.

| Test | Projectile | Matrix system | Projectile mass (g) | Impact velocity (m/s) | Impact energy (J) |
|---|---|---|---|---|---|
| GCP-I | Gelatine | PEEK | 20 ± 0.5 | 61 ± 2.5% | 37 ± 5% |
| GCE-I | Gelatine | Epoxy | 20 ± 0.5 | 62 ± 2.5% | 38 ± 5% |

**Table 7**
Results from the CF/PEEK and CF/Epoxy composites impacted by the gelatine projectiles.

| Test | Matrix system | Velocity (m/s) | Energy (J) | Maximum major strain | Maximum OOP displacement (mm) |
|---|---|---|---|---|---|
| GCP-I | PEEK | 61 ± 2.5% | 37 ± 5% | 0.013 ± 3% | 3.9 ± 3% |
| GCE-I | Epoxy | 62 ± 2.5% | 38 ± 5% | N/A | 4.0 ± 3% |

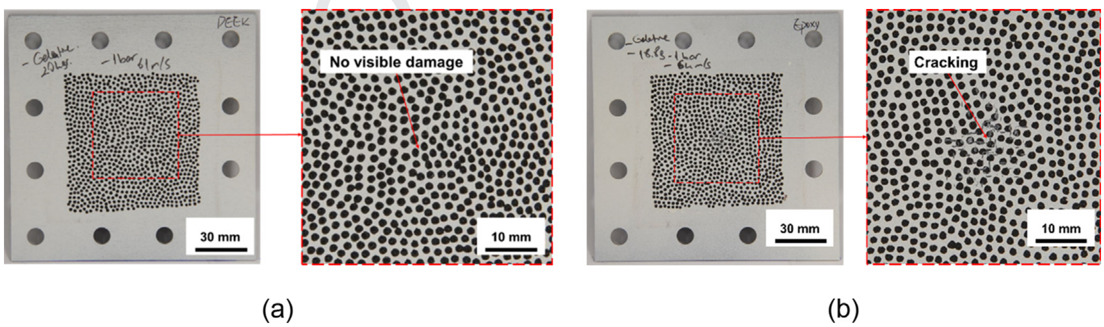


**Fig. 11.** The rear-faces of the specimens after impact: (a) the CF/PEEK composite impacted at a 37 J energy level and (b) the CF/epoxy composite impacted at a 38 J energy level.



Please cite this article as: H. Liu, J. Liu, C. Kaboglu et al., The behaviour of fibre-reinforced composites subjected to a soft impact-loading: An experimental and numerical study, Engineering Failure Analysis, https://doi.org/10.1016/j.engfailanal.2020.104448

## 6. The Finite element (FE) model

### 6.1. Model definition

As a discussed earlier, in order to model the soft-body impact on the composite test specimens a Finite-Element (FE) model was developed based upon a commercial software code, 'Abaqus/Explicit 2017'. Within the FE model, the gelatine projectile was modelled using the Smoothed Particle Hydrodynamics (SPH) modelling technique [18]. As discussed earlier, the SPH method is a meshless Lagrangian technique where the solid FE mesh for the gelatine impactor is replaced by a set of discrete interacting particles. The gelatine projectile was first modelled using 8-node linear-brick (C3D8R) elements. However, upon initial contact of the projectile with the composite target specimen, these elements were converted to continuum particle (PC3D) elements, see Fig. 12. The characteristic length for the PC3D elements was 0.5 mm, which was equivalent to half of the element size that was used for modelling the gelatine projectile with the CSD8R elements. The total mass of the projectile was equally distributed between all the 8-node linear-brick (C3D8R) elements or all the continuum particle (PC3D) elements. Turning to the modelling of the composite specimen, the damage theories discussed earlier [13–15] were originally developed for unidirectional fibre-reinforced composite plies. Hence, the [0–90°] woven carbon-fibre ply used for the CF/PEEK and CF/epoxy composites was represented as two unidirectional-fibre sub-plies, joined at right angles to the

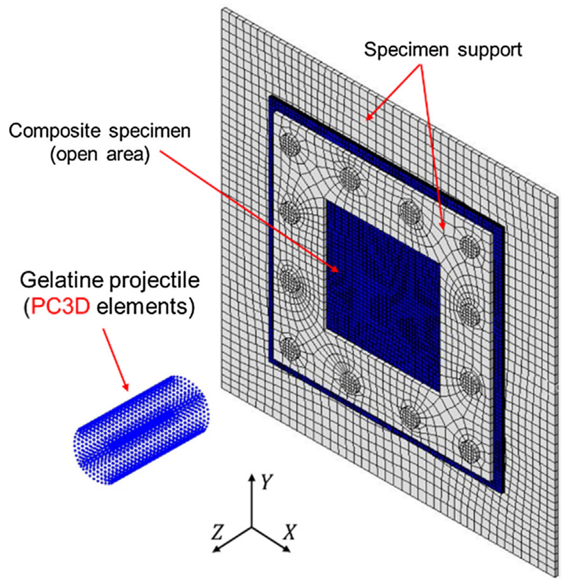


**Fig. 12.** The FE model with PC3D elements.

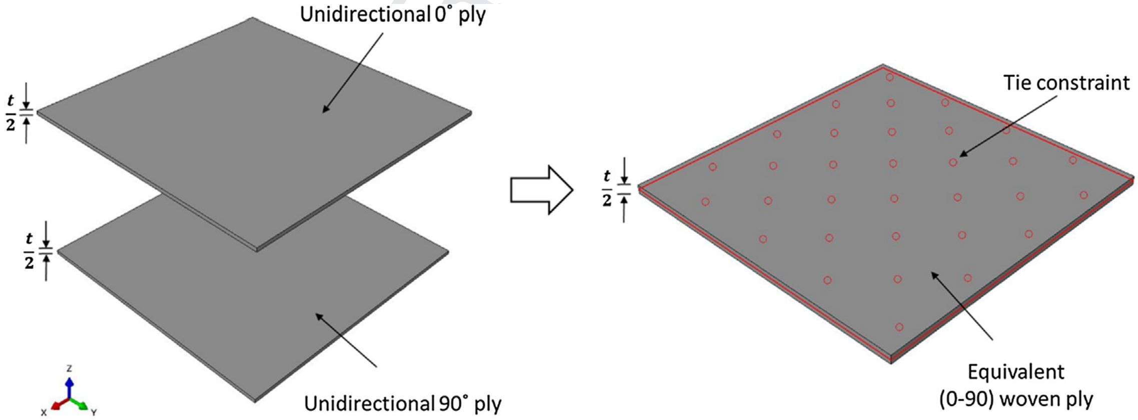


**Fig. 13.** The creation of a single equivalent [0°-90°] woven-fibre reinforced composite ply.

Please cite this article as: H. Liu, J. Liu, C. Kaboglu et al., The behaviour of fibre-reinforced composites subjected to a soft impact-loading: An experimental and numerical study, Engineering Failure Analysis, https://doi.org/10.1016/j.engfailanal.2020.104448

fibre direction. Thus, in the FE modelling, two unidirectional-fibre sub-plies were first created, with the thickness of each of the unidirectional-fibre sub-plies (i.e. 0.125 mm) being equal to half that of the thickness of the equivalent [0–90°] woven-fibre composite ply (i.e. 0.25 mm). These two unidirectional-fibre sub-plies were placed at right angles and then joined using 'tie constraints', to form a single equivalent [0–90°] woven-fibre composite ply, which has the same in-plane properties as the actual woven-fibre composite ply that was used in the composite specimens, see Fig. 13. The elements employed in the FE model for the composite target test specimens were 8-node quadrilateral in-plane general-purpose continuum shell (SC8R) elements, with an element size of 1 mm × 1 mm. The interfaces between the composite plies were modelled using the cohesive surface law, which is again a built-in sub-routine within the 'Abaqus/Explicit 2017' code [22–24]. The boundary conditions employed in the model were the same as those used in the gas-gun experiments. A general contact algorithm was used to govern the global contact in the numerical modelling and a friction coefficient of 0.2 was adopted for the global contact [25–27].

### 6.2. Input parameters

In order to use the SPH method for capturing the response of the soft-gelatine projectile, an equation of state (EOS) with suitable input parameters, as shown in Eqs. (5) and (6), is required for the modelling of the gelatine projectiles, see Section 2.1. The input parameters required for the numerical modelling of the gelatine projectiles are shown in Table 8. For the composite specimen, it was defined using continuum shell elements and only the in-plane material properties are then required for the numerical modelling. However, the values of the cohesive stiffness, maximum cohesive strength and the various fracture energies do need to be inputted into the sub-routine which simulates the damage evolution in the composite via a linear-softening material model embedded in a bilinear cohesive law. The relevant material properties of the CF/PEEK and CF/epoxy composites required for the FE modelling studies may be found from the literature [28–35] and are given in Table 9.

### 6.3. Implementation of the model

Fig. 14a shows the flow chart of the main FE model and Fig. 14b shows the sub-routine for the composite damage model. In the computation process a computation step was performed for every appropriate single element in the FE model. In the composite damage model, if any of the damage criteria are initiated, the model will then run the flow-path 'Yes', otherwise the flow-path 'No' will be taken. Note that the time associated with the impact event enters the FE model by the 'Model state' being equivalent to a 'step time'. The numerical model is stopped when the defined total time for the impact event has expired.

**Table 8**
Input properties for the FE modelling of the soft-gelatine projectile [37–39].

| Properties | Reference density | Dynamic viscosity | Reference speed of sound | Slope of the $U_s$ versus $U_p$ curve | Grüneisen ratio |
|---|---|---|---|---|---|
| Values | 1.06 $g/cm^3$ | $1 \times 10^{-6}$ MPa · s | $c_0 = 1.45 \times 10^6$ mm/s | $s = 1.87$ | $\Gamma = 1.09$ |

**Table 9**
Input properties for the FE modelling studies of the composite [28–35].

| Property | Unidirectional CF/PEEK sub-ply | Unidirectional CF/epoxy sub-ply |
|---|---|---|
| Moduli (GPa) | $E_{11} = 127$; $E_{22} = 10.3$; $G_{12} = 5.7$ | $E_{11} = 125$; $E_{22} = 8.7$; $G_{12} = 4.3$ |
| Poisson's ratio | $\nu_{12} = 0.3$ | $\nu_{12} = 0.3$ |
| Strength values (MPa) | $X^T = 2070$; $Y^T = 85$ | $X^T = 1930$; $Y^T = 41$ |
| | $X^C = 1360$; $Y^C = 276$ | $X^C = 1250$; $Y^C = 254$ |
| | $S^L = S^T = 186$; | $S^L = S^T = 110$ |
| Ply fracture energies ($kJ/m^2$) | $G_{Ic}\|_{ft} = 218$; $G_{Ic}\|_{fc} = 104$ | $G_{Ic}\|_{ft} = 201$; $G_{Ic}\|_{fc} = 92$; |
| | $G_{Ic}\|_{mt} = 1.7$; $G_{Ic}\|_{mc} = 2.0$ | $G_{Ic}\|_{mt} = 0.6$; $G_{Ic}\|_{mc} = 1.5$ |
| Interlaminar fracture energies⁺ ($kJ/m^2$) | $G_{Ic} = 1.7$; $G_{IIc} = 2.0$ | $G_{Ic} = 0.6$; $G_{IIc} = 1.5$ |
| Benzeggagh–Kenane mode-mix exponent⁺ | $\eta_{BK} = 1.09$ | $\eta_{BK} = 2.09$ |
| Initial cohesive law strength (MPa) | $t^0_{33} = 43$; $t^0_{31} = t^0_{32} = 50$ | $t^0_{33} = 20$; $t^0_{31} = t^0_{32} = 34$ |
| Initial cohesive law stiffness (N/mm) | $k = 6.4 \times 10^5$ | $k = 6.2 \times 10^5$ |

Note:
$G_{Ic}$ and $G_{IIc}$ are the Mode I and Mode II interlaminar fracture energies between two [0–90°] woven-fibre composite plies.
$G_{Ic}|_{ft}$ and $G_{Ic}|_{fc}$ are the tensile and compressive ply fracture energies of the unidirectional-fibre sub-plies in the longitudinal fibre-direction.
$G_{Ic}|_{mt}$ and $G_{Ic}|_{mc}$ are the tensile and compressive ply fracture energies of the unidirectional-fibre sub-plies in the transverse to fibre direction.
⁺ These properties are for interlaminar failure between two of the [0–90°] woven-fibre plies.



Please cite this article as: H. Liu, J. Liu, C. Kaboglu et al., The behaviour of fibre-reinforced composites subjected to a soft impact-loading: An experimental and numerical study, Engineering Failure Analysis, https://doi.org/10.1016/j.engfailanal.2020.104448

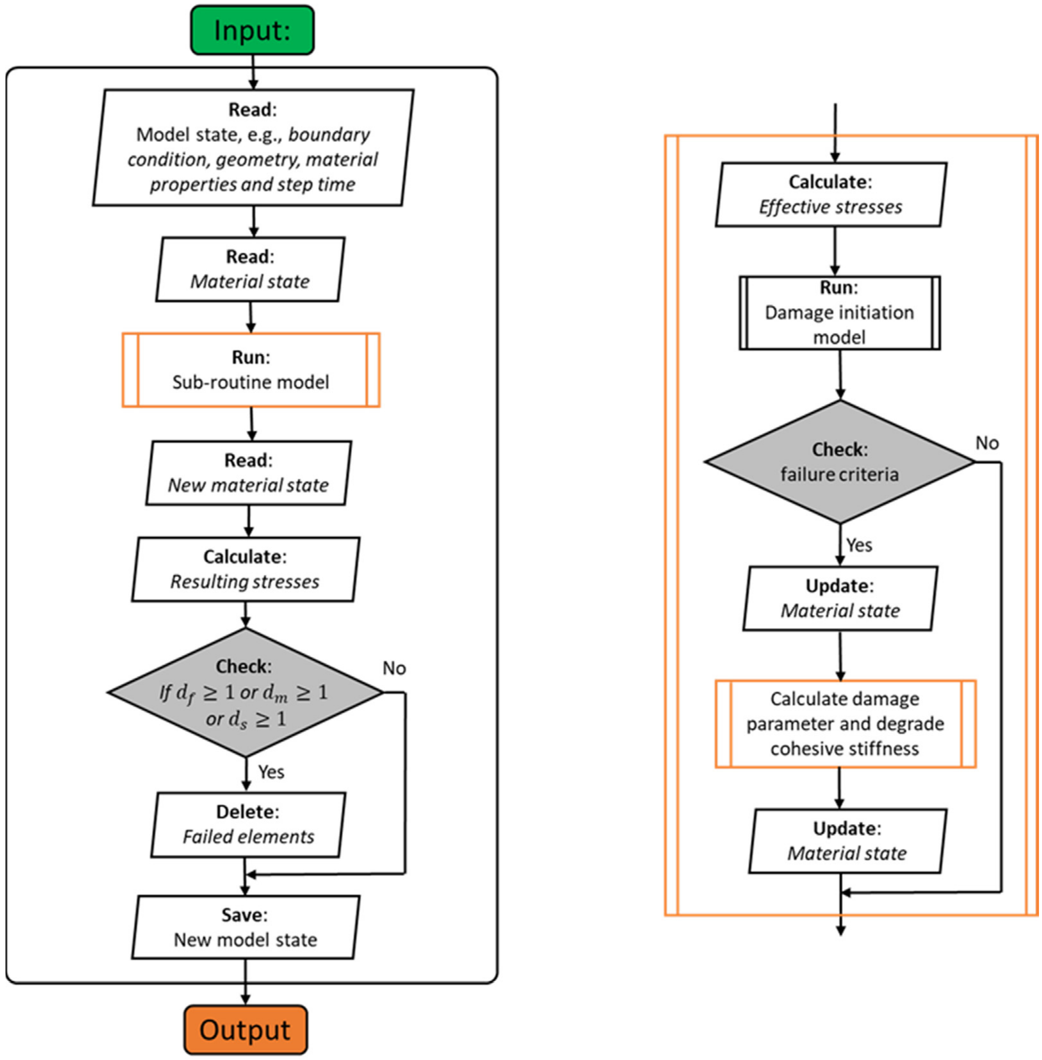


(a) (b)

**Fig. 14.** The implementation of the FE model showing schematically the flowcharts for one computation step for a single element: (a) the flowchart of the main model and (b) the flowchart of the sub-routine model for assessing the initiation and evolution of composite damage. Note that in (b) for the sub-routine model the failure criteria for the initiation and evolution of damage are given by Eqs. (8)–(15) for intralaminar damage and by Eq. (17) for interlaminar damage.

## 7. Model validation and application

### 7.1. Validation of the model

#### 7.1.1. The deformation of the gelatine projectile

The deformation histories of the gelatine projectile obtained from the experimental studies and predicted using the FE model for an impact test conducted at an energy level of 37 J on the CF/PEEK composite (i.e. 'Test GCP-I') are compared in Fig. 15. The experimental results show that, after the initial contact with the composite specimen, the front of the gelatine projectile started to deform and flow to the periphery of the composite specimen. Correspondingly, the modelling results show a similar phenomenon, as shown in Fig. 15b. At a later stage of the impact event, see Fig. 15e, most of the gelatine projectile has deformed, flowed and spread over the surface of the composite specimen, and again the modelling studies accurately capture this behaviour of the gelatine projectile. Thus, the comparison between the experimental and numerical modelling results reveal that the SPH model for the relatively soft-gelatine projectile can indeed reproduce the experimental behaviour of the soft-gelatine projectile used in the gas-gun impact experiments.

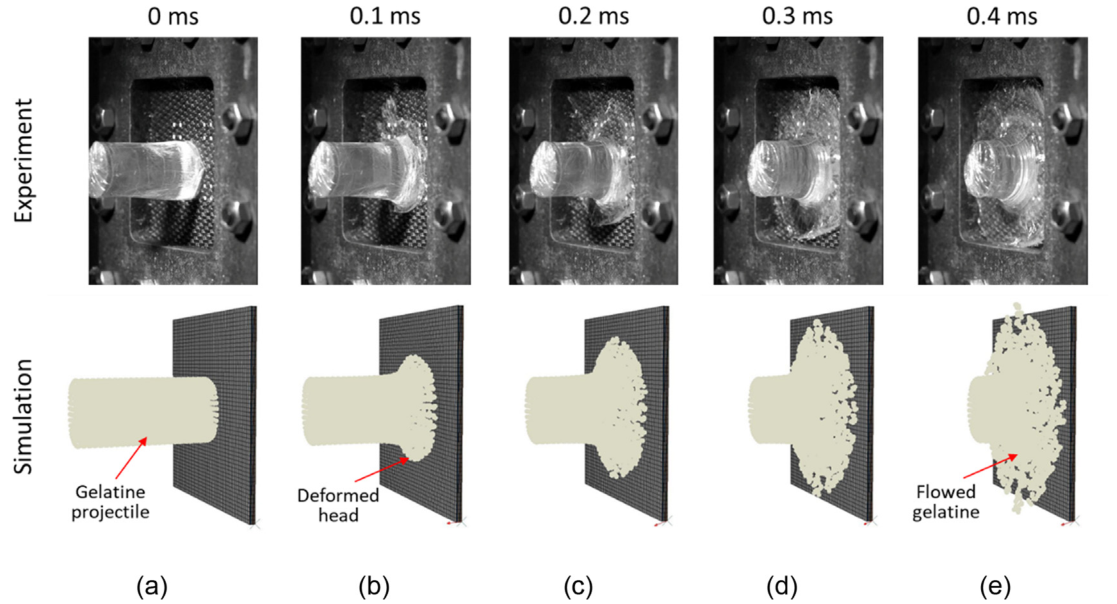


**Fig. 15.** Deformation of the gelatine projectile obtained from the experimental studies and as predicted from the numerical FE model for the CF/PEEK composites at an impact energy of 37 J.

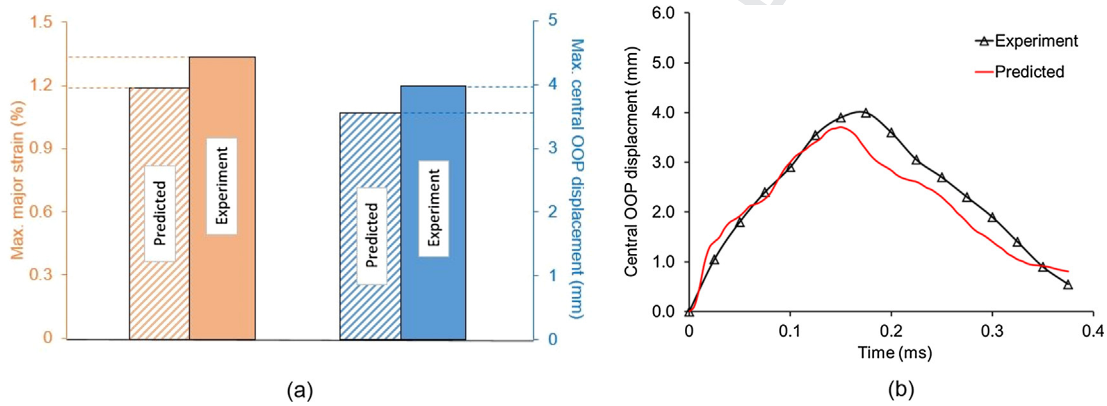


**Fig. 16.** Comparison between the predicted and experimental results for the CF/PEEK composite at an impact energy of 37 J: (a) the maximum major strain and the out-of-plane (OOP) displacement and (b) the central OOP displacement versus time trace.

### *7.1.2. The CF/PEEK composites*

Based on the DIC results obtained from the experiment conducted at an impact energy of 37 J using the gelatine projectile (i.e. 'Test GCP-I'), the major strain and out-of-plane (OOP) displacement histories of the centre point for the rear-face of the composite test specimen can be extracted. The values of the maximum major strain and central OOP displacement predicted from the FE modelling studies are compared with the corresponding experimental results in Fig. 16a, and good agreement may be seen. To further confirm the accuracy of the numerical FE model, the predicted central OOP displacement versus time trace was also compared with the corresponding experimental results, see Fig. 16b. It can be seen from these results that, although the modelling studies gave somewhat lower maximum values than the experimentally measured values, the general trend and overall response of the composites were predicted extremely well using the numerical FE model. The slightly lower prediction values may be due to curvature effects in the woven material which the model could not fully capture.

The next step is to assess the capability of the numerical FE model that has been developed to predict the impact damage created in the composite by the impact event, and two impact energies levels of 37 J and 72 J were so modelled. The experimental and predicted extents of damage at these two energy levels, which resulted in the CF/PEEK composites, are shown in Fig. 17a and b, respectively. (The 'DAMAGESHR' shown in the legend corresponds to the shear damage.) It was found that, at an energy level of 37 J, the prediction from the FE numerical modelling studies was that no visible impact damage would have been suffered by the composite specimen. This finding is in excellent agreement with the experimental results. When

Please cite this article as: H. Liu, J. Liu, C. Kaboglu et al., The behaviour of fibre-reinforced composites subjected to a soft impact-loading: An experimental and numerical study, Engineering Failure Analysis, https://doi.org/10.1016/j.engfailanal.2020.104448

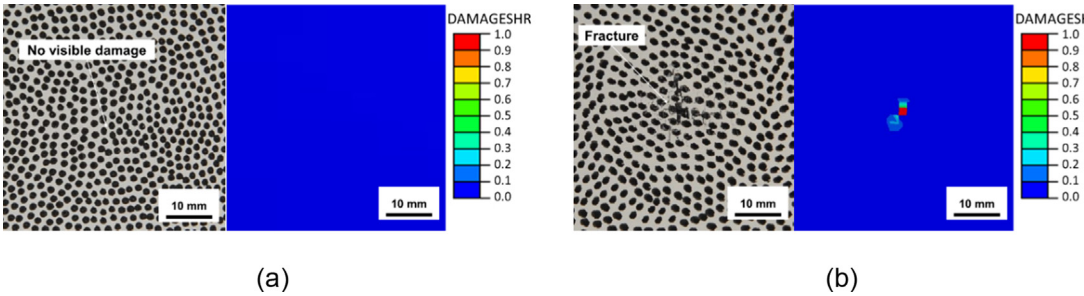


**Fig. 17.** The experimentally measured and predicted degrees of damage resulting in the rear-face of the CF/PEEK composites at impact energies of (a) 37 J and (b) 72 J.

an impact energy level of 72 J was modelled, failure was predicted to be present only in the central area of the CF/PEEK composite, as shown in Fig. 17b. The experimental results revealed that some damage had indeed occurred in this region of the composite. In addition, the extent of the damage, as determined from the post-impact experimental observations on this composite specimen, is accurately predicted by the numerical studies.

## 7.2. Application of the model

### 7.2.1. Predicting the deformation of the CF/PEEK and CF/epoxy composites

To model the effects of the matrix system on the impact response of the composites, the central OOP displacement was predicted from the FE model for the CF/PEEK specimens impacted at a 37 J energy level and the CF/epoxy specimens impacted at a 38 J energy level, as shown in Fig. 18a. The central OOP displacement versus time traces predicted for the CF/PEEK composite and for the CF/epoxy composite exhibited a very similar behaviour up to a peak value of the displacement followed by a gradual decrease. Fig. 18b shows a comparison of the maximum central OOP displacements predicted in the FE model for the CF/PEEK ('Test GCP-I' at 37 J) and the CF/epoxy ('Test GCE-I' at 38 J) composites. When impacted, the CF/epoxy composite ('Test GCE-I') is predicted from the FE modelling to undergo a maximum central OOP displacement of 3.9 mm, which is marginally higher than that of 3.7 mm for the CF/PEEK composite ('Test GCP-I'). These predicted values of the central OOP displacement for the two types of composite are also compared with the experimental results in Table 10, where very good agreement may be seen between the experimental measurements and the FE modelling simulations. The out of plane displacement response for CF/PEEK and CF/epoxy are very similar as both composites have the same carbon fibres with similar volume fraction.

### 7.2.2. Predicting the post-impact damage of the composites

A comparison of the post-impact damage in the composites obtained from the experiments and the FE numerical modelling results for the CF/PEEK and the CF/epoxy composites is shown in Fig. 19a and 19b, respectively. It can be seen that the

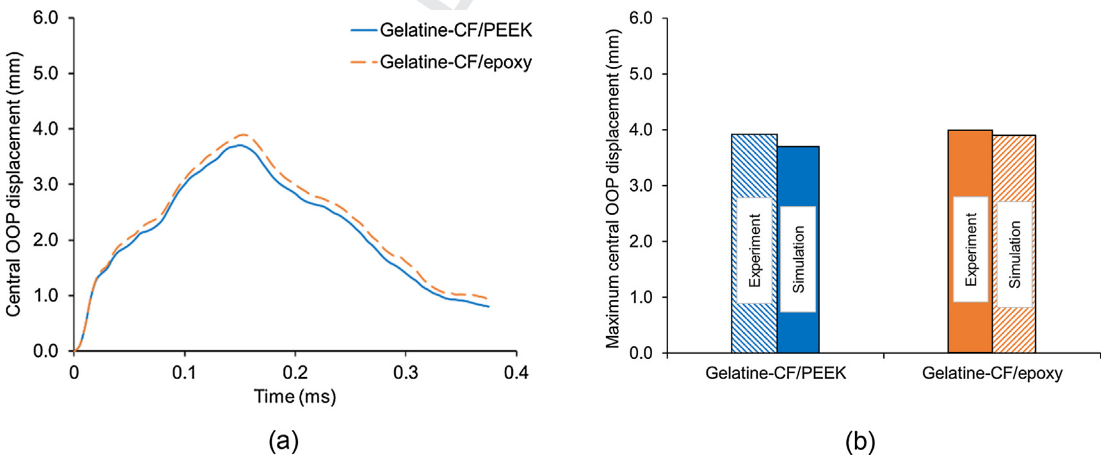


**Fig. 18.** Predicted (a) central out-of-plane (OOP) displacement versus time trace and (b) the experimentally measured and predicted maximum OOP displacements for the CF/PEEK impacted at 37 J and the CF/epoxy impacted at 38 J.

**Table 10**
Comparison of the experimentally measured and the numerically predicted maximum central out-of-plane (OOP) displacement.

| Composite | Energy level | Experiment ($d_e$) | Simulation ($d_m$) | Deviation $\left(\left\|\frac{d_m-d_e}{d_e}\right\| \times 100\%\right)$ |
|---|---|---|---|---|
| CF/PEEK | 37 J | 3.9 mm | 3.7 mm | 5.1% |
| CF/epoxy | 38 J | 4.0 mm | 3.9 mm | 2.5% |

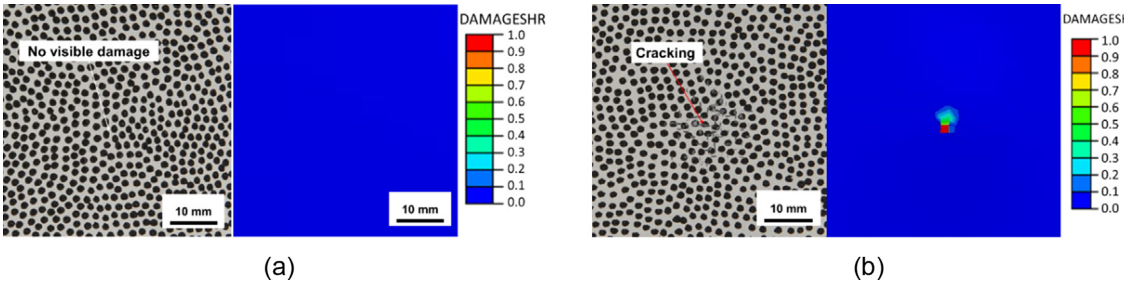


**Fig. 19.** Comparison of the damage obtained from the experiments and the FE modelling: (a) the CF/PEEK composite impacted at 37 J and (b) CF/epoxy composite impacted at 38 J.

predicted results for the CF/PEEK did not show any damage, which agrees fully with the experimental observations. On the other hand, the modelling results for the CF/epoxy predicted that some centrally-located damage would occur, which was indeed observed in the experimental studies. The evolution of damage was observed by plotting the derived damage variable, $d_s$, which is dependent on fibre and matrix failure, $d_f$ and $d_m$ respectively, as defined by Eq. (15). The damage observed in CF/epoxy on the rear face was mostly localised matrix and fibre failure at the centre of the panel. The amount of energy expended in damage of the composite sample for CF/PEEK and CF/epoxy was very small relative to the incident impact energy. Most of the incident impact energy is transformed into elastic energy in the specimen which is then dissipated in friction at the support fixtures and in intrinsic damping, as the specimen vibrates after impact. Of course, some of the incident impact energy is dissipated in plastic flow of the projectile.

*7.2.3. Predicting the contact pressure between the projectile and the composite*

The numerical FE model was also employed to predict the average contact pressure between the soft-gelatine projectile and the composite specimen by using Eq. (7), see Section 2.1. This parameter could not be readily experimentally measured in the gas-gun experiments. The contact pressure versus time histories were obtained from the FE models for (a) the CF/PEEK composite impacted at an impact energy of 37 J and (b) the CF/epoxy impacted an impact energy of 38 J, and the results are shown in Fig. 20a. It can be seen that the CF/PEEK and the CF/epoxy composites suffered a very similar average contact pressure history, with an initial short duration compressive phase giving rise to a relatively high initial contact pressure. The predicted maximum average contact pressures for the CF/PEEK and the CF/epoxy impact tests, when the relatively soft-gelatine projectile was used, are 10.7 MPa and 9.8 MPa, respectively, as shown in Fig. 20b.

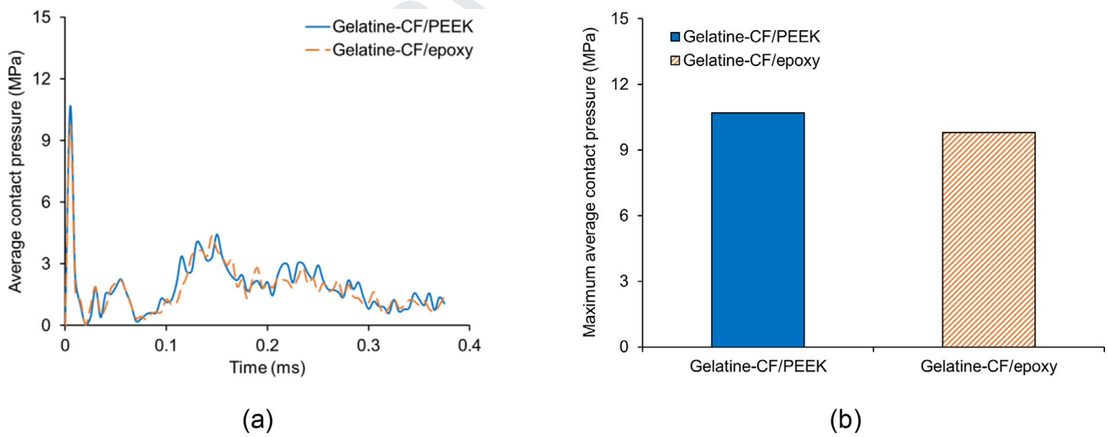


**Fig. 20.** Numerical predictions from the FE model for: (a) the average contact pressure versus time history and (b) the maximum average contact pressure. (For the CF/PEEK composite impacted at an energy of 37 J and (b) the CF/epoxy impacted an energy of 38 J.

Please cite this article as: H. Liu, J. Liu, C. Kaboglu et al., The behaviour of fibre-reinforced composites subjected to a soft impact-loading: An experimental and numerical study, Engineering Failure Analysis, https://doi.org/10.1016/j.engfailanal.2020.104448

## 8. Conclusions

This paper has focussed on experimental and numerical studies of the response of polymer-matrix fibre-reinforced composites under impact loading by a soft projectile. A simple but reliable technique was proposed for the preparation of the relatively soft-gelatine projectiles and a plastic sabot was employed to maintain the shape of the gelatine projectile upon being launched from the gas-gun. A high-speed camera was used to record the deformation of the projectile during the impact event. The recorded frames showed that the gelatine projectile behaved as a viscoelastic-plastic fluid. The gas-gun tests were firstly performed using woven carbon-fibre reinforced poly(ether-ether ketone) (CF/PEEK) composite specimens, using the gelatine projectiles, at four different impact energy levels. Secondly, to investigate the effects of the matrix system on the impact response of the composites, woven carbon-fibre reinforced epoxy (CF/epoxy) were impacted using the gelatine projectiles. The experimental results demonstrated that the CF/epoxy composite exhibited a lower impact resistance and suffered more impact damage, compared with the CF/PEEK composite, when struck by the gelatine projectiles using a similar impact energy.

A finite-element (FE) numerical model was developed, which was based on the 'Abaqus/Explicit 2017' commercially-available software code, for predicting the behaviour of the projectile and the composite test specimen during the impact event. The FE numerical model has enabled (a) the deformation, (b) the initiation of damage, and (c) the evolution of such damage in the composite target specimens to be predicted, as well as the deformation and flow behaviour (and the contact pressure) of the projectile. The results from the numerical studies have been found to be in very good agreement with the experimental results.

In terms of design, woven architectures are often employed on the outside of composite laminates to generate a hybrid architecture. Woven composites do not have the stiffness of an equivalent laminate carbon-fibre material but they have the advantage that delamination and interfacial cracking does not occur so readily as has been shown by the above modelling and experiments. CF/PEEK is a very attractive woven material as the threshold for damage is higher than an equivalent CF/epoxy and this has also been confirmed by the modelling and experiments.

## Uncited references

[19,21].

## Declaration of Competing Interest

The authors declare that they have no known competing financial interests or personal relationships that could have appeared to influence the work reported in this paper.

## Acknowledgements

This paper was presented at the 3rd International Conference on Structural Integrity, 2nd–5th September 2019, Funchal, Madeira organised by Professor Pedro Moreira and Professor Paulo Tavares. The strong support from the Aviation Industry Corporation of China (AVIC), Manufacturing Technology Institute (MTI), the First Aircraft Institute (FAI) and the Aircraft Strength Research Institute (ASRI) for this funded research is much appreciated. The research was performed at the AVIC Centre for Structural Design and Manufacture at Imperial College London, UK.

## References

[1] Savage G, Bomphray I, Oxley M. Exploiting the fracture properties of carbon fibre composites to design lightweight energy absorbing structures. Eng. Fail. Anal. 2004;11:677–94.
[2] Curtis PT, Bader MG, Bailey JE. The stiffness and strength of a polyamide thermoplastic reinforced with glass and carbon fibres. J. Mater. Sci. 1978;13:377–90.
[3] Tsai SW, Hahn T. Introduction to Composite Materials Science. Routledge; 2018.
[4] Siegmann A, Ben-Tzur M. Tensile behaviour of thermoplastic. J. Mater. Sci. 1987;22:1405–12.
[5] Opelt CV, Cândido GM, Rezende MC. Fractographic study of damage mechanisms in fiber reinforced polymer composites submitted to uniaxial compression. Eng. Fail. Anal. 2018;92:520–7.
[6] Rolfe E, Quinn R, Sancho A, Kaboglu C, Johnson A, Liu H, Hooper PA, Dear JP, Arora H. Blast resilience of composite sandwich panels with hybrid glass-fibre and carbon-fibre skins. Multiscale Multidiscip. Model. Exp. Des. 2018;1:197–210.
[7] Liu H, Falzon BG, Tan W. Predicting the Compression-After-Impact (CAI) strength of damage-tolerant hybrid unidirectional/woven carbon-fibre reinforced composite laminates. Compos. Part A Appl. Sci. Manuf. 2018;105:189–202.
[8] Bibo GA, Hogg PJ. The role of reinforcement architecture on impact damage mechanisms and post-impact compression behaviour. J. Mater. Sci. 1996;31:1115–37.
[9] Bogenfeld R, Kreikemeier J, Wille T. Review and benchmark study on the analysis of low-velocity impact on composite laminates. Eng. Fail. Anal. 2018;86:72–99.
[10] Heimbs S, Bergmann T. High-Velocity Impact Behaviour of Prestressed Composite Plates under Bird Strike Loading. Int. J. Aerosp. Eng. 2012;2012:1–11.
[11] Zbrowski A. Experimental tests concerning the impact resistance of a tailplane. Arch. Civ. Mech. Eng. 2014;14:53–60.
[12] Johnson AF, Holzapfel M. Numerical prediction of damage in composite structures from soft body impacts. J. Mater. Sci. 2006;41:6622–30.
[13] Hashin Z, Rotem A. A Fatigue Failure Criterion for Fiber Reinforced Materials. J. Compos. Mater. 1973;7:448–64.
[14] Hashin Z. Failure criteria for unidirectional fiber composites. J. Appl. Mech. 2015;47:329–34.
[15] Abaqus 2017 documentation, Dassault Systèmes, Provid. Rhode Island, USA, 2017.

[16] Zhou SG, Sun CT. Failure analysis of composite laminates with free edge. J. Compos. Tech. Res. 1990;12:91–7.
[17] Turon A, Dávila CG, Camanho PP, Costa J. An engineering solution for mesh size effects in the simulation of delamination using cohesive zone models. Eng. Fract. Mech. 2007;74:1665–82.
[18] Johnson AF, Holzapfel M. Modelling soft body impact on composite structures. Compos. Struct. 2003;61:103–13.
[19] Liu H, Liu J, Kaboglu C, Chai H, Kong X, Blackman BRK, Kinloch AJ, Dear JP. Experimental and numerical studies on the behaviour of fibre-reinforced composites subjected to soft impact loading. Procedia Struct. Integr. 2019;17:992–1001.
[20] Chiu LNS, Falzon BG, Ruan D, Xu S, Thomson RS, Chen B, Yan W. Crush responses of composite cylinder under quasi-static and dynamic loading. Compos. Struct. 2015;131:90–8.
[21] Liu H, Falzon BG, Dear JP. An experimental and numerical study on the crush behaviour of hybrid unidirectional/woven carbon-fibre reinforced composite laminates. Int. J. Mech. Sci. 2019;164:105160.
[22] Tan W, Falzon BG. Modelling the crush behaviour of thermoplastic composites. Compos. Sci. Technol. 2016;134:57–71.
[23] Faggiani A, Falzon BG. Predicting low-velocity impact damage on a stiffened composite panel. Compos. Part A Appl. Sci. Manuf. 2010;41:737–49.
[24] J. Liu, H. Liu, C. Kaboglu, X. Kong, Y. Ding, H. Chai, B.R.K. Blackman, A.J. Kinloch, John P. Dear, (3) (PDF) The impact performance of woven-fabric thermoplastic and thermoset composites subjected to high-velocity soft and hard impact loading. Available from: https://www.researchgate.net/publication/335421994_The_impact_performance_of_woven-fabric_ther 2019.
[25] Liu H, Falzon BG, Catalanotti G, Tan W. An experimental method to determine the intralaminar fracture toughness of high-strength carbon-fibre reinforced composite aerostructures. Aeronaut. J. 2018;122:1352–70.
[26] Falzon BG, Liu H, Tan W. Comment on A tensorial based progressive damage model for fiber reinforced polymers. Compos. Struct. 2017;176:877–82.
[27] Radchenko A, Radchenko P. Numerical modeling of development of fracture in anisotropic composite materials at low-velocity loading. J. Mater. Sci. 2011;46:2720–5.
[28] Liu H, Falzon BG, Tan W. Experimental and numerical studies on the impact response of damage-tolerant hybrid unidirectional/woven carbon-fibre reinforced composite laminates. Compos. Part B Eng. 2018;136:101–18.
[29] Liu H, Falzon BG, Li S, Tan W, Liu J, Chai H, Blackman BRK, Dear JP. Compressive failure of woven fabric reinforced thermoplastic composites with an open-hole: an experimental and numerical study. Compos. Struct. 2019;213:108–17.
[30] CYTEC, APC-2-PEEK Thermoplastic Polymer, 2012. https://www.cytec.com/sites/default/files/datasheets/APC-2_PEEK_031912-01.pdf.
[31] Naderi M, Khonsari MM. Stochastic analysis of inter- and intra-laminar damage in notched PEEK laminates. Express Polym. Lett. 2013;7:383–95.
[32] M. V Donadon, B.G. Falzon, L. Iannucci, J.M. Hodgkinson, Measurement of fibre fracture toughness using an alternative specimen geometry, in: Proc. 16th Int. Conf. Compos. Mater. July 2007, Kyoto, Japan, 2007.
[33] Kim JK, Sham ML. Impact and delamination failure of woven-fabric composites. Compos. Sci. Technol. 2000;60:745–61.
[34] Iannucci L, Willows ML. An energy based damage mechanics approach to modelling impact onto woven composite materials — Part I: Numerical models. Compos. Part A Appl. Sci. Manuf. 2006;37:2041–56.
[35] Turon A, Camanho PP, Costa J, Renart J. Accurate simulation of delamination growth under mixed-mode loading using cohesive elements: Definition of interlaminar strengths and elastic stiffness. Compos. Struct. 2010;92:1857–64.
[36] Hou JP, Ruiz C. Soft body impact on laminated composite materials. Compos. Part A Appl. Sci. Manuf. 2007;38:505–15.
[37] Frissane H, Taddei L, Lebaal N, Roth S. SPH modeling of high velocity impact into ballistic gelatin. Development of an axis-symmetrical formulation. Mech. Adv. Mater. Struct. 2018;3:1–8.
[38] Abdul Kalam S, Vijaya Kumar R, Ranga Janardhana G. SPH high velocity impact analysis-influence of bird shape on rigid flat plate. Mater. Today Proc. 2017;4:2564–72.
[39] Georgiadis S, Gunnion AJ, Thomson RS, Cartwright BK. Bird-strike simulation for certification of the Boeing 787 composite moveable trailing edge. Compos. Struct. 2008;86:258–68.



Please cite this article as: H. Liu, J. Liu, C. Kaboglu et al., The behaviour of fibre-reinforced composites subjected to a soft impact-loading: An experimental and numerical study, Engineering Failure Analysis, https://doi.org/10.1016/j.engfailanal.2020.104448